Bioorganic Chemistry **30,** 107–118 (2002)
doi:10.1006/bioo.2002.1239, available online at http://www.idealibrary.com on IDEAL®

Use of Kinetic Isotope Effects to Delineate the Role of Phenylalanine 87 in $P450_{BM-3}$

Dan A. Rock, Anthony E. Boitano, Jan L. Wahlstrom, Denise A. Rock, and Jeffrey P. Jones[1]

Department of Chemistry, Washington State University, Pullman, Washington 99164

Received August 13, 2001

The substrate oxidation rates of $P450_{BM-3}$ are unparalleled in the cytochrome P450 (CYP) superfamily of enzymes. Furthermore, the bacterial enzyme, originating from *Bacillus megaterium*, has been used repeatedly as a model to study the metabolism of mammalian P450s. A specific example is presented where studying $P450_{BM-3}$ substrate dynamics can define important enzyme–substrate characteristics, which may be useful in modeling ω-hydroxylation seen in mammalian P450s. In addition, if the reactive species responsible for metabolism can be controlled to produce specific products this enzyme could be a useful biocatalyst. Based on crystal structures and the fact that the $P450_{BM-3}$ F87A mutant produces a large isotope in contrast to the native enzyme, we propose that phenylalanine 87 is responsible for hindering substrate access to the active oxygen species for nonnative substrates. Using kinetic isotopes and two aromatic substrates, *p*-xylene and 4,4′-dimethylbiphenyl, the role phenylalanine 87 plays in active-site dynamics is characterized. The intrinsic KIE is 7.3 ± 2 for *wt*$P450_{BM-3}$ metabolism of *p*-xylene. In addition, stoichiometry differences were measured with the native and mutant enzyme and 4,4′-dimethylbiphenyl. The results show a more highly coupled substrate/NADPH ratio in the mutant than in the *wt*$P450_{BM-3}$.

Key Words: P450BM-3; kinetic isotope effects (KIE); stoichiometry; ω-hydroxylation; biocatalyst.

INTRODUCTION

In general, cytochrome P450 enzymes can perform a variety of difficult chemistries. For example, they can oxidize unfunctionalized hydrocarbons (*1*). These chemistries have important roles in industrial processes and drug metabolism. Cytochrome $P450_{BM-3}$ originates from the soil bacterium, *Bacillus megaterium*. The bacterial $P450_{BM-3}$ possesses unique characteristics when compared to the superfamily of enzymes: (i) it can metabolize substrates much faster than other P450s, with oxidation rates as high as 4600 nmol/min/nmol P450 (*2*) and, (ii) the heme and FAD/FMN reductase of $P450_{BM-3}$ are fused together forming a large 119-kDa enzyme. The latter

[1] To whom correspondence should be addressed at PO Box 644630, Pullman, WA 99164-4630. Fax: (509) 335-8867. E-mail: jpj@wsu.edu.

0045-2068/02 $35.00

attribute is partly responsible for the increased rates, as the required collision event between the heme and the reductase prior to electron transfer is eliminated. Furthermore, the nature of the reductase classifies $P450_{BM-3}$ as a type II P450, grouping it with mammalian P450s. As such, the bacterial enzyme has often been used to model the metabolism of mammalian P450s. Such models are useful, especially when the P450 isoforms have similar metabolic profiles for a given set of substrates (*3*). For instance, the eukaryotic 4F family metabolizes long-chain fatty acids at the omega position (*4,5*) while $P450_{BM-3}$, also has a high degree of specificity for long-chain fatty acids, but produces only internal alcohols and no ω-hydroxylation in the wild-type enzyme (*4,6*)

The versatility of $P450_{BM-3}$ enables the study of this enzyme to overlap multiple disciplines: (i) to better understand the metabolism of endogenous chemicals in mammals by P450s and, (ii) to develop the catalytic powers of this enzyme for biocatalysis. (i) As stated, $P450_{BM-3}$ shows tendencies to metabolize similar substrates to the P450 4F family and shares the same sites of metabolic activity toward long-chain fatty acids. With a more complete understanding of $P450_{BM-3}$ dynamics, this system may be used to model the metabolic activity of the P450 4F family. (ii) Alternatively, defining the dynamics of substrate metabolism is important in the development of this enzyme as a biocatalyst and would allow the powerful oxidant and fast rates to be more fully utilized.

Several crystal structures of $P450_{BM-3}$ have been solved, with and without substrates bound (*7–9*). As a result, certain residues have been identified that directly participate in the binding of substrates once in the active site. Specifically, phenylalanine 87 has been shown to be in close contact with the heme on the distal side of the binding pocket, adjacent to the I-helix. This occupies a great deal of the active site as shown in Fig. 1A. To study the impact of phenylalanine 87 on substrate metabolism, residue 87 was mutated to alanine (*10*). $P450_{BM-3}$ F87A becomes an ω-hydroxylase, where the terminal carbon of the fatty acid becomes the principal metabolite much like that seen for the 4F family. This contrasts with *wt*$P450_{BM-3}$, where metabolism occurs only at the internal carbons of fatty acids. The measured difference in reactivity between these two positions indicates that without enzyme–substrate interactions, the omega-1 position would be favored over the omega position by a factor of 25 to 1 (*4,11*). The outcome shows that the mutant favors the least activated position for hydrogen atom abstraction, implying that in the F87A mutant the terminal methyl group can approach more closely to the active oxygen species when compared to the internal hydrogen atoms. By studying $P450_{BM-3}$ enzyme–substrate interactions, we hope to gain insight into why P450 4F metabolism occurs at the omega position.

The enzyme dynamics described above are also important in the development of enzymes for benign synthesis, biocatalysis, and bioremediation (*12*). The cytochrome P450 superfamily of enzymes is able to oxidize a range of structurally diverse organic compounds. In fact, substrate binding does not appear to reduce the transition-state energy for the hydrogen atom abstraction event in P450 enzymes (*12*). Therefore, substrate binding can result in multiple orientations producing numerous metabolites from a single substrate. The powerful oxidant responsible for hydrogen atom abstraction and subsequent oxidation in P450s is generally thought to be the iron–oxene species (*13, 14*). This highly reactive intermediate is capable of oxidizing most any

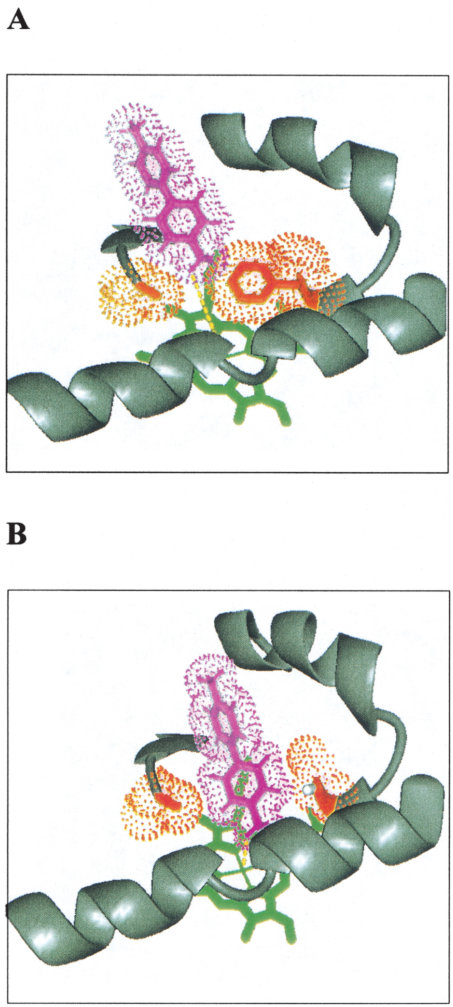

FIG. 1. The crystal structure of P450$_{BM-3}$ was taken from the Protein Data Bank. Subsequent docking of substrate, 4,4-dimethylbiphenyl was performed using Midas (San Francisco, CA). The substrate and enzyme were minimized using Amber 6 (UCSF, CA). van der Waal radii are highlighted. (**A**) From left to right, A328, 4,4-dimethylbiphenyl, and F87 are highlighted and show the high level of contact between F87 and 4,4-dimethlybiphenyl. (**B**) The F87A mutant increases substrate access to the heme.

hydrocarbon and is the reason why multiple products form. To develop P450s as biocatalysts, the enzyme dynamics must be more fully understood in order to limit binding orientations and to enhance a specific metabolic product.

The importance of understanding P450$_{BM-3}$ enzyme dynamics has been established, but methods used to identify enzyme–substrate interactions are limited and difficult. Several techniques in enzymology have been developed to study enzyme activity. The use of kinetic isotope effect experiments has been successful at determining complicated interactions associated with substrate motion in the active site of certain

enzymes (*3,15,16*). To measure the enzyme dynamics using KIE it is necessary to first estimate the intrinsic isotope effect. As described by Northrop (*17*), an intrinsic isotope effect will be observed in an intramolecular experiment if interchange between the enzyme–substrate complexes that lead to either hydrogen or deuterium abstraction is rapid. For the substrate shown in Fig. 2A this only requires rotation about a carbon–carbon single bond.

Since single bond rotation is fast, this type of experiment will almost always lead to an intrinsic isotope effect (*18,19*). A second intramolecular experiment can be used to measure the limit of dynamic motion associated with the substrate in the active site of an enzyme. Specifically, using a chemical that possesses a C_2 axis of symmetry such as the compounds shown in Fig. 2B, where one end of a molecule is deuterated and the other end possesses protons. In this case, reorientation of the entire molecule is required in order to produce the KIE_{intr} (Fig. 2B). If substrate reorientation is slow, the observed isotope effect will be smaller than the intrinsic isotope effects, but if reorientation is fast, the observed isotope effect will equal the intrinsic isotope effect.

To test the active-site dynamics of $P450_{BM-3}$ and the F87A mutant we choose to use kinetic isotope effect experiments with two intramolecular probes shown in Scheme 1, *p*-xylene **1** and 4,4′-dimethylbiphenyl **2** (*18*). Specifically, we hypothesize that the F87A mutant will allow the substrate to reorient faster in the active site. To test this hypothesis we will use the well-defined substrate probes to identify the capacity of substrate rotation and translation within the active site of $P450_{BM-3}$ and the F87A mutant enzyme.

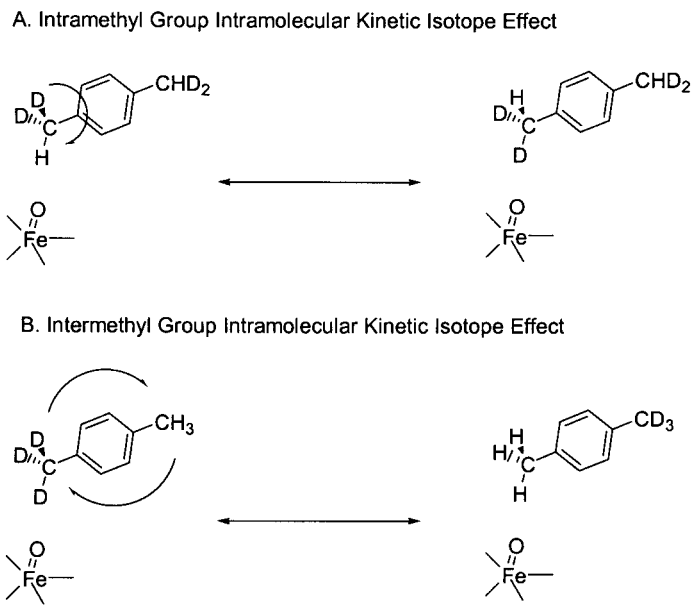

FIG. 2. The cartoon shows the difference between the (A) intramethyl KIE and the (B) inter-Methyl KIE.

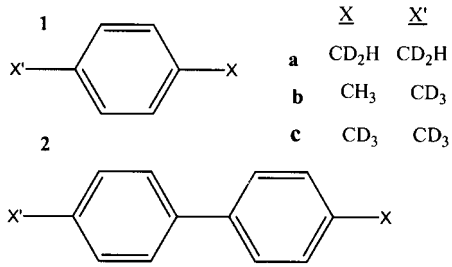

SCHEME 1. Cytochrome P450 substrates used for the measurement of isotope effects.

METHODS AND MATERIALS

Materials and Reagents

p-Xylene and 4,4′-dimethylbiphenyl were purchased from Aldrich (Milwaukee, WI). G-6-P, G-6-P dehydrogenase, catalase, and NADPH were purchased from Sigma (St. Louis, MO). MTBSTFA was purchased from Regis Technologies, Inc. (Morton Grove, IL). DH5α competent cells were purchased from Gibco Life Technologies (Gaithersburg, MD). Site-directed mutagenesis was performed with the Quick Change site directed mutagenesis kit from Stratagene (La Jolla, CA). All solvents were purchased from J. T. Baker, Inc. (Phillipsburg, NJ). The remaining reagents were of the highest purity commercially available. Spectroscopic studies were performed on a SLM Aminco DW-2000 UV-VIS spectrophotometer. Oxygen consumption data were recorded with an iso-750 Clark-type oxygen probe from World Precision Instruments (Sarasota, FL). Proton NMR was obtained at 300 MHz on a Varian instrument. Site-directed mutagenesis was confirmed by sequencing in the molecular research facility LBB1 of Washington State University.

Expression

Recombinant P450$_{BM-3}$ from *B. megatarium* was expressed in DH5α *Escherichia coli* cells as described (*20*). Yields of pure protein after 2′, 5′-ADP column (*21*,*22*) were 200–300 nmol per liter of growth media. The protein was pure and homogenous as determined by SDS-PAGE. The concentration of protein was determined using the molar extinction coefficient 96 mM^{-1} cm^{-1} (*23*). Enzyme stocks were run through a PD-10 column (Sephadex G25 resin) equilibrated with 0.1 M potassium phosphate buffer (pH 7.4) to remove 2,3-AMP, concentrated and frozen at −80°C prior to use.

Synthesis of Substrates

(A) p-Xylene-α-$^2H_3$. *p*-Methyltoluate (5.2 g, 0.036 mol) in 20 mL of anhydrous diethyl ether was added drop wise to lithium aluminum detrude (1.6 g, 0.04 mol) suspended in 50 mL of anhydrous diethyl ether. The reaction was stirred at room temperature for 3 h under argon atmosphere and then quenched with 1 mL of ice, 2 mL of 15% sodium hydroxide, and with another 2 mL of water cautiously. The solution was filtered and the filtrate was rinsed with cold diethyl ether. The solution was then extracted 2 × 75 mL of pentane. The pentane was dried over magnesium

sulfate and concentrated under reduced pressure to yield *p*-methyl benzyl alcohol (3.8 g, 0.031, 90%). The resulting *p*-xylene was >99% pure by GC and by MS had a deuterium content of 98.20 at.% deuterium-d_3, 1.59 at.% deuterium-d_2, and negligible d_1 and d_0.

(B) Synthesis of p-Xylene-α-$^2H_2$-α'-$^2H_2$. Terephthalic acid (2.76 g, 0.015 mol) was added dropwise to lithium aluminum deuteride (1.2 g, 0.03 mol) suspended in 60 mL of ether. The reaction was stirred overnight and then terminated with 1 mL of ice while reaction was stirred in an ice bath. Followed by 1.2 mL of 3 M NaOH and 1.2 mL of water. The resulting mixture was filtered and the ether was then rinsed 2 × 50 mL of water. The remaining ether layer was dried over magnesium sulfate, filtered, and evaporated to yield 0.97 g (0.007 mol) of clear diol. The product was then stirred with 10 mL of 48% hydrobromic acid for 30 min. The resulting solid was recrystallized and filtered to yield 0.5 g (0.002 mol) of grayish-white solid. The dibromo product was suspended in minimal dimethyl sulfoxide and then added to a stirring solution of sodium borohydride (0.25 g, 0.006 mol) in 10 mL of dimethyl sulfoxide. After 12 h, 40 mL of pentane was added followed by the careful addition of 10 mL of water. The mixture was then carefully rinsed with 2 × 25 mL of water. The remaining pentane was dried over sodium sulfate and then evaporated. The resulting α-$^2H_2$-α'-$^2H_2$-*p*-xylene was applied to column chromatography over neutral silica and carefully evaporated and the corresponding fractions were stored in −80°C refrigerator until use, as these products are volatile. The resulting *p*-xylene was pure by GC and by MS had a deuterium content of 97.71 at.% deuterium-d_4, 1.64 at.% deuterium-d_3, and 0.65 at.% deuterium-d_2.

(C) 4′-Methylbiphenyl-4-carboxylic acid. 4,4′-Dimethylbiphenyl (2.3 g, 0.013 mol) was suspended in 100 mL of glacial acetic acid and 4.6 g (0.05 mol) of chromium trioxide was carefully added. The mixture was slowly heated and maintained at 90°C for 2 h. Then the reaction was allowed to cool before adding to 500 mL of ice-cold water. The green solution was filtered and washed with ice water until the precipitate was colorless. The precipitate was dissolved in 2 M ammonia in methanol, filtered, and then reprecipitated by acidifying with 75% hydrochloric acid solution. The precipitate was filtered and dried yielding (0.6 g, 0.003 mol) of 4′-methylbiphenyl-4-carboxylic acid.

(D) Synthesis of 4-$^2H_3$,4′-dimethylbiphenyl. To lithium aluminum deuteride (210 mg, 0.005 mol) suspended in 50 mL of dry tetrahydrofuran, 4′-methylbiphenyl-4-carboxylic acid (0.5 g, 0.0024 mol) was added slowly. The reaction was stirred for 16 h under argon. The reaction was terminated with 1 mL of ice, 1 mL of 15% sodium hydroxide, and 2 mL of water. The mixture was then filtered, dried over magnesium sulfate, and evaporated, yielding a crude oil. The product alcohol was purified by silica gel (12 g) column chromatography with chloroform:methanol (9:1) as eluant. The alcohol (310 mg, 0.0016 mol) was dissolved in dichloromethane and reacted with *p*-toluenesulfonyl chloride (380 mg, 0.0020 mol) and triethylamine (1 mL) for 48 h. The mixture was washed with 2 × 75 mL water and dried over sodium sulfate and evaporated to yield the tosylated product. The product was purified by silica gel (5 g) column chromatography with pentane as an eluant. The tosylate (65 mg, 0.2 mmol) was reduced with lithium aluminum deuteride (0.1 g, 0.003 mol) to yield 4-$^2H_3$,4′-dimethylbiphenyl. This compound was purified by silica gel (25 g)

column chromatography with pentane as the eluant. The resulting dimethylbiphenyl was >99% pure by GC and by MS had a deuterium content of 94.42 at.% deterium-d_3, 4.46 at.% deuterium-d_2, 0.389 at.% deuterium-d_1, and 0.297 at.% deuterium-d_0.

(E) Synthesis of 4-$^2H_2$,H,4′-$^2H_2$,H-dimethylbiphenyl. This compound was prepared according to the same procedure as that described for (B) except that the methyl ester of biphenyl-4,4′-dicarboxylic acid was used as the starting material.

Incubations

Incubations were performed in 1–mL volume; 1 nmol P450, 5–10 μL (50 mM substrates A, B, D, E), 910–950 μL of 0.1 M potassium phosphate buffer (pH, 7.4), and initiated with 10 μL (20 mM NADPH). Incubations were performed at 30°C, for 20 min prior to extraction with 2 × 2 mL pentane. The pentane layers were combined and concentrated and the samples were then derivatized with MtBSTFA overnight prior to analysis on the GC/MS.

Stoichiometry

The molar extinction coefficient for NADPH is 6220 M^{-1} cm^{-1} at 340 nm and was used to measure NADPH consumption rates with ultraviolet spectroscopy. Simultaneously oxygen consumption was monitored with a Clark-type electrode. A reaction volume of 1.7 mL was used to ensure that no air transfer could take place after the lid was placed on a 1.7-mL cuvette. The reaction mixture comprised amounts equivalent to those of the incubations described above. Postincubation, 40 μL of sample was aliquoted into 400 μL of a standard solution of zylenol orange (Pierce Chemicals, Rockford, IL). After 15 min the absorbance at 560 nm was measured and compared to a standard curve in order to determine the peroxide content of each reaction. The remaining reaction was stopped with the addition of 2 mL of pentane after 10 min, spiked with internal standard, extracted, and analyzed using GC/MS.

GC/MS Analysis

GC/MS analysis was performed on a Finnigan Voyager GC/MS, fitted with a 30 m Hewlett Packard DB-5 fused silica capillary column, and operated in the selected ion-monitoring mode. The derivatized xylenes were cold-trapped at 40°C, and the temperature was raised linearly at 15°C/min to 135°C followed by isothermal elution for 5 min. For the derivatized biphenyls an initial temperature of 100°C was used for 1 min, followed by a linear ramp at 15°C/min to 250°C, and completed by isothermal elution for 5 min. The $[M - 57]^+$ ion of the silyl derivative was monitored for the various xylene isomer metabolites and 4,4′-dimethylbiphenyl metabolites. Mass spectral conditions were as follows: 50 ms dwell time, −70 eV ionizing voltage, and 200–205°C source temperature. Deuterium incorporation in each substrate was determined using the same GC parameters as those used for each of the respective metabolites or by bleeding the compound through the reference inlet. The mass spectral conditions were the same as those used for the metabolites except that the ionizing voltage was −12.5 eV. The measured ion intensity of each ion was corrected for the natural isotopic abundance of ^2H, ^{13}C, ^{14}C, ^{18}O, and ^{29}Si (*31*).

RESULTS

$P450_{BM-3}$ and the F87A mutant were used to metabolize α-$^2H_2$-α'-$^2H_2$-*p*-xylene **1a** to determine the isotope effect. The results will estimate the intrinsic isotope effect for benzylic hydroxylation by *wt*$P450_{BM-3}$ and the F87A mutant as described by Higgins *et al.* (*24*). No detectable amount of phenol oxidation was observed, therefore, benzylic oxidation was the only product. The $k_H/k_{D\ obs}$ is obtained by taking the ratio of hydrogen-abstracted benzylic oxidation product to the deuterium-abstracted hydroxylation product. The uneven distribution of protons on each methyl is then statistically corrected. The $k_H/k_{D\ obs}$ for *wt*$P450_{BM-3}$, under these conditions, was 7.3 ± 0.2 and 8.2 ± 0.1 for the $P450_{BM-3}$ F87A mutant (Table 1). The large isotope effects suggest fast rotation of the benzylic methyl group of *p*-xylene. Consequently, these isotope effects should closely approximate the intrinsic isotope effects.

A similar intra-methyl group isotope effect experiment was performed with 4-$^2H_2$,4′-$^2H_2$′-dimethylbiphenyl **2a** and the intrinsic isotope effects associated with the benzylic oxidation were determined. The $k_H/k_{D\ obs}$ for biphenyl is 6.8 ± 0.2 for *wt*$P450_{BM-3}$ as shown in Table 1. The $P450_{BM-3}$ F87A mutant yielded an observed isotope effect of 7.8 ± 0.3. Again the methyl group rotation appears to be fast, yielding the unmasked isotope effect with respect to *wt*$P450_{BM-3}$ and 4,4′-dimethylbiphenyl as the substrate.

The metabolism of α-$^2H_3$-*p*-xylene **1b** by $P450_{BM-3}$ yields two possible products since no phenol product is observed. Substrate **1b** has protons on one methyl, while the opposite methyl has three deuteriums. This experiment is distinguished from the intra-methyl group isotope effect by the fact that differential hydroxylation of *p*-xylene (3 deuteriums and 3 protons) requires a rapid reorientation of the entire molecule in order to express the intrinsic isotope effect (Fig. 2B). Substrate **1b** was used in incubations for both *wt*$P450_{BM-3}$ and the $P450_{BM-3}$ F87A mutant. The $k_H/k_{D\ obs}$ from benzylic hydroxylation was 9.8 ± 0.3 and 9.1 ± 0.1, respectively (Table 1). These values indicate that reorientation of *p*-xylene is fast, and the isotope effect is unmasked in *wt*$P450_{BM-3}$ and the F87A mutant enzyme. In contrast, a small isotope effect would indicate substrate reorientation within the active site of the enzyme to be slow. The same experiments were repeated with 4-$^2H_3$,4-H-dimethylbiphenyl **2b** and *wt*$P450_{BM-3}$ and the F87A mutant. An isotope effect of 2.5 ± 0.4 was observed for *wt*$P450_{BM-3}$ and **2b**. However, the F87A mutant yields an observed isotope effect of 7.2 ± 0.2 with **2b** as the substrate. The isotope effect difference between the wild-type and the F87A mutant reveals that the mutant facilitates substrate mobility as

TABLE 1

Kinetic Isotope Effects for *p*-Xylene and 4,4′-Dimethylbiphenyl

	p-Xylene		4,4′-Dimethylbiphenyl	
CYP	**1a**	**1b**	**2a**	**2b**
$P450_{BM-3}$	7.3 (2)	9.8 (3)	6.8 (4)	2.5 (4)
$P450_{BM-3}$F87A	8.2 (1)	9.1 (1)	7.8 (4)	7.2 (2)

indicated by the large isotope effect (Table 1). Therefore, reorientation is fast in the F87A mutant for **2b**, but not for the wild-type enzyme.

Alternatively, the expressed isotope effects could result from the breakdown of the enzyme-substrate complex prior to oxidation where the substrate could rebind in a position necessary to metabolize the nondeuterated methyl. This event would produce an isotope effect, but yield little information about substrate dynamics within the active site. To test this possibility a competitive intermolecular kinetic isotope effect experiment can be used to determine the contribution of substrate debinding to the observed isotope effect. We measured the intermolecular KIE for the F87A mutant using compound **2C**. The resulting isotope effect, 1.03 ± 0.1, shows substrate debinding to be slow. As such, the changes in the intramolecular KIE reflect the change in the substrates ability to rotate within the active site of the mutant relative to the wild-type enzyme.

Rates for NADPH and oxygen consumption were measured as describe under Methods and Materials, as well as peroxide and product formation. The data (Table 2) reveal distinct differences between the *wt*P450$_{BM-3}$ and the P450$_{BM-3}$ F87A mutant. The rates of NADPH consumption are faster for the mutant when compared to *wt*P450$_{BM-3}$, 10.0 and 4.4, respectively. Furthermore, the F87A mutant produces more product and less hydrogen peroxide when compared to *wt*P450$_{BM-3}$. In addition, the Product/NADPH ratios, which in a highly coupled P450 reaction should equal one, indicate *wt*P450 is more uncoupled with respect to 4,4′-dimethylbiphenyl.

DISCUSSION

P450$_{BM-3}$ enzyme–substrate interactions can increase our ability to understand *in vivo* metabolism. This holds true for cases where the compared P450s share a common substrate and show similar metabolic profiles such as P450$_{BM-3}$ F87A and P450 4F family. In addition, such interactions are crucial to technological advances associated with bioremediation and benign synthesis with respect to cytochrome P450s. Therefore, this work attempts to define the active-site dynamics of P450$_{BM-3}$, specifically aiming to identify the role of phenylalanine 87 in substrate metabolism. Active-site residues like phenylalanine 87 that actively participate in substrate binding must be defined to develop an ability to predict the regioselectivity of substrate metabolism by P450. In this report, *p*-xylene and 4,4′-dimethylbiphenyl were chosen as substrate probes that possess two benzylic hydroxylation sites separated by at least one aromatic ring, in order to monitor substrate dynamics.

TABLE 2

Stoichiometry for 4,4′-Dimethylbiphenyl and P450$_{BM-3}$F87A

Enzyme	NADPH[a]	Oxygen	Product	H_2O_2	NADPH/O_2	Product/ NADPH	H_2O_2/ NADPH
P450$_{BM-3}$	5.7 (1)[b]	4.4 (4)	0.31 (3)	0.98 (2)	1.3	0.052	0.17
P450$_{BM-3}$F87A	10.0 (1)	9.2 (3)	0.66 (2)	0.12 (4)	1.1	0.065	0.01

[a] All products in nmol/min/nmol.

[b] Indicates the standard deviation (SD) in the last significant digit in the value.

The isotope effects reported in Table 1 show that *wt*P450$_{BM-3}$ and P450$_{BM-3}$ F87A accommodate rapid motion in the active site with respect to *p*-xylene **1a** and **1b**. Substrate reorientation within the active site is confirmed by the expression of the intrinsic isotope effects. Whereas, the isotope effects for 4,4′-dimethylbiphenyl **2b** reveal that the substrate does not reorient rapidly in *wt*P450$_{BM-3}$ as suggested by the masked isotope effect of 2.5 ± 0.4. The small isotope effect of 2.5 for *wt*P450$_{BM-3}$ and 4,4′-dimethylbiphenyl **2b** substrate is attributed to the ability of phenylalanine 87 to hinder substrate motion (Fig. 1A). However, mutation of the active-site residue phenylalanine 87 to alanine opens the active site to accommodate rotation of the larger 4,4′-dimethylbiphenyl substrate (Fig. 1B). The ability to reorient is confirmed by the large isotope effects seen with 4,4′-dimethylbiphenyl **2b** and the F87A mutant.

Based on X-ray crystallography structures and the fact that the F87A mutant produces a large isotope effect in contrast to the wild-type enzyme, we propose that phenylalanine 87 is responsible for the hindered substrate motion, as it occupies a large amount of the active site. Furthermore, phenylalanine 87 may decrease the number of times the substrate collides with the iron−oxene species. That is, the bulky phenyl ring of residue 87 prevents the substrate from contacting the iron-oxene species. In contrast, replacement of phenylalanine 87 with alanine results in a large isotope effect as a result of a more accessible active site. Other reports have confirmed that the F87A mutant increases the ability of substrates like laurate to bind more specifically to P450$_{BM-3}$ (*10*).

To further explore the steric effects in the active site of P450$_{BM-3}$ we measured the stoichiometry of the P450 reaction cycle to identify the effects of limited substrate access caused by phenylalanine 87. The efficiency of a P450 reaction is defined by the amount of product formed relative to the amount of NADPH consumed. For a tightly coupled system the product/NADPH consumption equals one. The three initial steps of the reaction cycle have the most dramatic affect on P450 stoichiometry. The reaction cycle begins upon substrate binding and the exclusion of water from the active site. This initial step allows the heme to then accept electrons from the reductase. Therefore, substrate binding directly influences the amount of water present in the active site. In general, a tightly bound substrate excludes water from the active site and has a more favorable reduction potential, when compared to a loosely bound substrate (*25*). Introduction of molecular oxygen is the next step leading to the iron−superoxide species. A second electron reduction can then take place. Again, the presence of water in the active site is important since water can influence the fate of the newly formed iron−hydroperoxy species. Specifically, if water is present in the active site then the iron−hydroperoxy species can release hydrogen peroxide. This results in uncoupling of NADPH and product in the P450 reaction cycle.

Peroxide formation and NADPH consumption for *wt*P450$_{BM-3}$ and P450$_{BM-3}$ F87A with respect to laurate were previously shown not to deviate from one another (*10*). This could be attributed to the size of laurate and the flexibility of phenylalanine 87 to orient together in an ordered fashion between the aromatic ring of phenylalanine 87 and the heme. Thus, both the F87A mutant and the *wt*P450$_{BM-3}$ enzyme enable laurate to bind close to the heme and exclude water. However, the aromatic substrates used here interact with the aromatic ring of phenylalanine 87 and limit access to the active site. In our experiments, P450$_{BM-3}$ F87A shows increased NADPH consumption

rates. The heme is more accessible to the substrates and, therefore, can more readily initiate electron transfer by excluding active-site waters as Fig. 1B illustrates. This also has the effect of decreasing hydrogen peroxide formation relative to *wt*P450$_{BM-3}$.

From the results it would appear that substrates **1** and **2** are excluded from the active site by F87 in the wild-type enzyme in the resting state. This decreases the overall rate of NADPH consumption. Furthermore, after the enzyme is reduced more hydrogen peroxide is released for this substrate than with the *wt* enzyme. This is most likely a result of disordered water protonating the iron–hydroperoxy species proximal to the iron. For the mutant, less hydrogen peroxide and more product is formed since the substrate is more likely to remain close to the heme which then excludes disordered waters and increases heterolytic cleavage to the iron–oxene species.

CONCLUSION

p-Xylene and 4,4′-dimethylbiphenyl were chosen to look at rotational motion in the active site of P450$_{BM-3}$. The use of KIEs coupled with the aromatic substrates produced valuable information regarding the enzyme–substrate complex found in P450$_{BM-3}$ during metabolism. These studies conclude that the P450$_{BM-3}$ F87A mutant enhances the binding of the above aromatic substrates in the active site of P450$_{BM-3}$ and consequently produces a more efficient reaction cycle for benzylic hydroxylation. Specifically, phenylalanine 87 restricts access to the active site of *wt*P450$_{BM-3}$ and limits reasonable substrate binding. The stoichiometry further shows that site-directed mutations can alter the P450 reaction cycle and enhance catalytic activities with respect to benign synthesis. While this paper has explained certain interactions in P450$_{BM-3}$ it also raised further questions which we are actively pursuing with modeling, isotope effects, and the use of natural fatty acids substrates in order to further develop our understanding of P450s.

ACKNOWLEDGMENT

We thank NIEHS ES 09122 for the support of this work.

REFERENCES

1. Groves, J. T., McClusky, G. A., White, R. E., and Coon, M. J. (1978) *Biochem. Biophys. Res. Commun.* **81,** 154–160.
2. Narhi, L. O., and Fulco, A. J. (1986) *J. Biol. Chem.* **261,** 7160–7169.
3. Jones, J. P., Korzekwa, K. R., Rettie, A. E., and Trager, W. F. (1986) *J. Am. Chem. Soc.* **108,** 7074–7078.
4. CaJacob, C. A., Chan, W. K., Shephard, E., and Ortiz de Montellano, P. R. (1988) *J. Biol. Chem.* **263,** 18640–18649.
5. Bambal, R. B., and Hanzlik, R. P. (1996) *Arch Biochem. Biophys.* **334,** 59–66.
6. Ho, P. P., and Fulco, A. J. (1976) *Biochim. Biophys. Acta* **431,** 249–256.
7. Boddupalli, S. S., Hasemann, C. A., Ravichandran, K. G., Lu, J. Y., Goldsmith, E. J., Deisenhofer, J., and A., P. J. (1992) *Proc. Natl. Acad. Sci. USA* **89,** 5567–5571.
8. Li, H. Y., Narasimhulu, S., Havran, L. M., Winkler, J. D., and Poulos, T. L. (1995) *J. Am. Chem. Soc.* **117,** 6297–6299.
9. Ravichandran, K. G., Boddupalli, S. S., Hasemann, C. A., Peterson, J. A., and Deisehofer, J. (1993) *Science* **261,** 731–736.
10. Oliver, C. F., Modi, S., Sutcliffe, M. J., Primrose, W. U., Lian, L. Y., and Roberts, G. C. (1997) *Biochemistry* **36,** 1567–1572.
11. Jones, J. P., Rettie, A. E., and Trager, W. F. (1990) *J. Med. Chem.* **33,** 1242–1246.

12. Jones, N. E., England, P. A., Rouch, D. A., and Wong, L. L. (1996) *Chem. Commun.* 2413–2414.
13. Jones, J. P., Rettie, A. E., and Trager, W. F. (1990) *J. Med. Chem.* **33,** 1242–1246.
14. Karki, S. B., Dinnocenczo, J. P., Jones, J. P., and Korzekwa, K. R. (1995) *J. Am. Chem. Soc.* **117,** 3657–3664.
15. Miwa, G. T., Garland, W. A., Hodshon, B. J., and Lu, A. Y. H. (1980) *J. Biol. Chem.* **255,** 6049–6054.
16. Hanzlik, R. P., Hogberg, K., Moon, J. B., and Judson, C. M. (1985) *J. Am. Chem. Soc.* **107,** 7164–7167.
17. Northrop, D. B. (1975) *Biochemistry* **14,** 2644–2651.
18. Iyer, K. R., Jones, J. P., Darbyshire, J. F., and Trager, W. F. (1997) *Biochemistry* **36,** 7136–7143.
19. Karki, S. B., and Dinnocenzo, J. P. (1995) *Xenobiotica* **25,** 711–724.
20. Higgins, L., Bennett, G. A., Shimoji, M., and Jones, J. P. (1998) *Biochemistry* **37,** 7039–7046.
21. Wen, L. P., and Fulco, A. J. (1987) *J. Biol. Chem.* **262,** 6676–6682.
22. Rock, D., Rock, D., and Jones, J. P. (2001) *Protein Expression Purif.* **22,** 82–83.
23. Omura, T., and Sato, R. (1964) *J. Biol. Chem.* **239,** 2370–2378.
24. Higgins, L., Korzekwa, K. R., Rao, S., Shou, M., and Jones, J. P. (2001) *Arch. Biochem. Biophys.* **385,** 220–230.
25. Ortiz de Montellano, P. R. (1995) Cytochrome P450:Structure, Mechanism, and Biochemistry, Plenum, New York.